Chemistry of Metal−Bound Anion Radicals. A Family of Mono- and Bis(azopyridine) Chelates of Bivalent Ruthenium

ARTICLE *in* INORGANIC CHEMISTRY · OCTOBER 2000

Impact Factor: 4.76 · DOI: 10.1021/ic000356b · Source: PubMed

4 AUTHORS, INCLUDING:

Kausikisankar Pramanik
Jadavpur University
42 PUBLICATIONS **445** CITATIONS
SEE PROFILE

Indranil Bhattacharyya
Narasinha Dutt College
1 PUBLICATION **34** CITATIONS
SEE PROFILE

Chemistry of Metal-Bound Anion Radicals. A Family of Mono- and Bis(azopyridine) Chelates of Bivalent Ruthenium

Maya Shivakumar, Kausikisankar Pramanik, Indranil Bhattacharyya, and Animesh Chakravorty*

Department of Inorganic Chemistry, Indian Association for the Cultivation of Science, Calcutta 700 032, India

Received April 4, 2000

The reaction of the dihydride $[Ru^{II}(H)_2(CO)(PPh_3)_3]$, **3**, with excess azo-2,2′-bipyridine (abp) in boiling dry benzene has afforded the diradical bischelate $[Ru^{II}(abp^{\bullet-})_2(CO)(PPh_3)]$, **4**, and the hydridic monochelate monoradical $[Ru^{II}(abp^{\bullet-})(H)(CO)(PPh_3)_2]$, **5**. A similar reaction between **3** and 2-(*p*-chlorophenylazo)pyridine (Clpap) did not yield a bischelate, but the hydridic monoradical $[Ru^{II}(Clpap^{\bullet-})(H)(CO)(PPh_3)_2]$, **6**, has been isolated. Upon treatment of **4**−**6** with NH_4PF_6 in a wet dichloromethane−acetonitrile medium, the one-electron-oxidized salts $\mathbf{4}^+PF_6^-$, $\mathbf{5}^+PF_6^-$, and $\mathbf{6}^+PF_6^-$ are isolated, H^+ being the oxidizing agent. The X-ray structures of $\mathbf{4}^+PF_6^-\cdot CH_2Cl_2$, $\mathbf{5}^+PF_6^-\cdot H_2O$, and $\mathbf{6}^+PF_6^-$ have been determined. In the monoradical $\mathbf{4}^+$ the azo N−N bond lengths in the two chelate rings are 1.284(6) and 1.336(6) Å, showing that the radical electron is localized in the latter ring. The half-filled extended Hückel HOMO is indeed found to be so localized, and it has a large azo character. Complexes **4**−**6** display radical redox couples with $E_{1/2}$ in the range −0.5 to +0.10 V vs SCE. The $E_{1/2}$ values qualitatively correlate with corresponding ν_{CO} values (1900−2000 cm^{-1}). The monoradicals ($S = {}^1/_2$) $\mathbf{4}^+$, **5**, and **6** uniformly display a strong EPR signal near $g = 2.00$. Metal-mediated magnetic interaction makes the EPR-silent diradical **4** strongly antiferromagnetic with $J = -299$ cm^{-1}. Crystal data are as follows: ($\mathbf{4}^+PF_6^-\cdot CH_2Cl_2$, $C_{40}H_{33}Cl_2F_6N_8OP_2Ru$) monoclinic, space group $P2_1/c$ (no. 14), $a = 14.174(6)$ Å, $b = 16.451(4)$ Å, $c = 18.381(4)$ Å, $\beta = 98.00(3)°$, $Z = 4$; ($\mathbf{5}^+PF_6^-\cdot H_2O$, $C_{47}H_{41}F_6N_4O_2P_3Ru$) monoclinic, space group $P2_1/n$ (no. 14), $a = 9.433(2)$ Å, $b = 38.914(17)$ Å, $c = 13.084(3)$ Å, $\beta = 103.47(2)°$, $Z = 4$; ($\mathbf{6}^+PF_6^-$, $C_{48}H_{39}ClF_6N_3OP_3Ru$) monoclinic, space group $P2_1/n$ (no. 14), $a = 10.496(5)$ Å, $b = 22.389(8)$ Å, $c = 19.720(6)$ Å, $\beta = 90.53(3)°$, $Z = 4$.

Introduction

The low-lying nature of the π^*-orbital makes the azo function susceptible to facile one-electron reduction, eq 1, in both free

$$\underset{(\sigma^2\pi^2)}{-N{=}N-} + e \rightarrow \underset{(\sigma^2\pi^2\pi^{*1})}{-N\cdots N-^-} \qquad (1)$$

and coordinated states. Generation of anion radical species by such reduction in solution has been documented for a long time,[1−4] but their isolation in the pure state was achieved only very recently.[5−9] We have demonstrated that the reaction of monohydrides of the type $[M^{II}(H)(X)(CO)(PPh_3)_3]$ (M = Ru, Os; X = Cl, Br) with azo heterocyclic ligands (general abbreviation L) in dry hydrocarbon solvents is attended with homolytic M−H cleavage, generating the chelated anion radical ligand $L^{\bullet-}$, eq 2. Crystalline species of the type $[M^{II}(L^{\bullet-})(X)(CO)(PPh_3)_2]$ have been isolated in this manner.[5−7]

Chart 1

1 azo-2, 2'-bipyridine (abp)

2 *p*-(chlorophenylazo)pyridine (Clpap)

3 $Ru^{II}(H)_2(CO)(PPh_3)_3$

4 $Ru^{II}(abp^{\bullet-})_2(CO)(PPh_3)$

$\mathbf{4}^+$ $Ru^{II}(abp^{\bullet-})(abp)(CO)(PPh_3)^+$

5 $Ru^{II}(abp^{\bullet-})(H)(CO)(PPh_3)_2$

$\mathbf{5}^+$ $Ru^{II}(abp)(H)(CO)(PPh_3)_2^+$

6 $Ru^{II}(Clpap^{\bullet-})(H)(CO)(PPh_3)_2$

$\mathbf{6}^+$ $Ru^{II}(Clpap)(H)(CO)(PPh_3)_2^+$

$$M^{II}H + L \rightarrow M^{II}L^{\bullet-} + {}^1/_2H_2 \qquad (2)$$

The above development has prompted us to explore the reaction between L and dihydridic $M^{II}(H)_2$ species with the objective of observing and isolating bischelated radical moieties such as $M^{II}(L^{\bullet-})_2$ and $M^{II}(L)(L^{\bullet-})$. This has been successfully achieved in the case of bivalent ruthenium. The intermediate

(1) Jonson, C. J.; Chang, R. *J. Chem. Phys.* **1965**, *43*, 3183.
(2) Sadler, J. L.; Bard, A. J. *J. Am. Chem. Soc.* **1968**, *90*, 1979.
(3) Goswami, S.; Mukherjee, R.; Chakravorty, A. *Inorg. Chem.* **1983**, *22*, 2825.
(4) Krause, R. A.; Krause, K. *Inorg. Chem.* **1984**, *23*, 2195.
(5) Shivakumar, M.; Pramanik, K.; Ghosh, P.; Chakravorty, A. *Inorg. Chem.* **1998**, *37*, 5968.
(6) Shivakumar, M.; Pramanik, K.; Ghosh, P.; Chakravorty, A. *Chem. Commun.* **1998**, 2103.
(7) Pramanik, K.; Shivakumar, M.; Ghosh, P.; Chakravorty, A. *Inorg. Chem.* **2000**, *31*, 195.
(8) Schwach, M.; Hausen, H.-D.; Kaim, W. *Inorg. Chem.* **1999**, *38*, 2242.
(9) Doslik, N.; Sixt, T.; Kaim, W. *Angew. Chem.* **1998**, *110*, 2125; *Angew. Chem., Int. Ed. Engl.* **1998**, *37*, 2403.

10.1021/ic000356b CCC: $19.00
Published on Web 08/25/2000

monohydridic monochelate radical system $Ru^{II}(H)(L^{\bullet-})$ has also been characterized. The structure and properties of representative members of this remarkable family of compounds are scrutinized in the present work.

Results and Discussion

A. Synthesis. a. Radical Species. The azo heterocyclic ligands **1** and **2**, the hydridic starting material **3**, and the isolated radical (**4**−**6** and $\mathbf{4}^+$) and nonradical ($\mathbf{5}^+$ and $\mathbf{6}^+$) species are listed in Chart 1. The structural drawings **4**−**6** shown below are based on definitive structural work (vide infra) and logical comparisons. In these drawings only the azo (N_a) and pyridine (N_p) nitrogen atoms of the $L^{\bullet-}$ ligand are shown.

Upon reaction of the dihydride **3**[10] with a 3-fold excess of abp in boiling dry benzene under nitrogen, a green solution is formed from which the diradical bischelate **4** incorporating

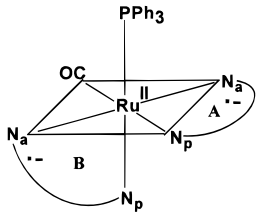

4

chelate rings A and B was isolated in good yield as a dark colored solid. In this synthesis the solvent and the reaction environment should be free of moisture; otherwise the monoradical $\mathbf{4}^+$ (see below) is formed as a contaminant.

When **3** and abp were reacted as above but with a smaller excess of abp, the hydridic monochelate monoradical **5** ac-

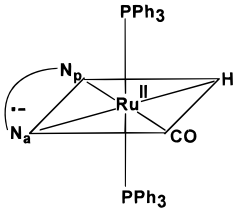

5

cumulated in solution and could be isolated, though in relatively poor yield. The radical-forming transformations involved in the synthesis of **4** and **5** are summarized in eq 3.

$$\underset{\mathbf{3}}{Ru(H)_2} \xrightarrow{abp} \underset{\mathbf{5}}{Ru(abp^{\bullet-})(H)} \xrightarrow{abp} \underset{\mathbf{4}}{Ru(abp^{\bullet-})_2} \qquad (3)$$

The reaction between **3** and excess Clpap failed to afford any tractable bischelate radical complex probably due to the weaker π-acceptor ability of Clpap compared to abp. However, the hydridic monoradical **6** could be isolated in which the coordination sphere is geometrically isomeric with that in **5**.

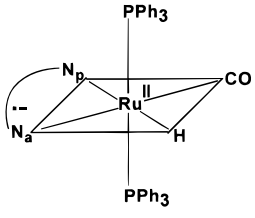

6

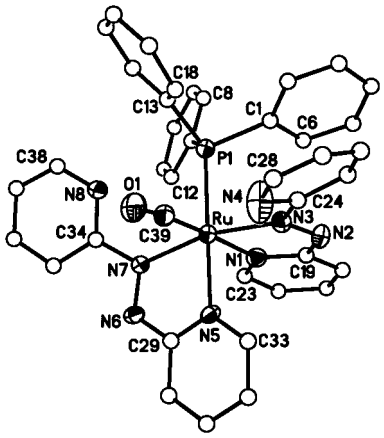

Figure 1. Molecular structure of the cation $[Ru^{II}(abp)(abp^{\bullet-})(CO)(PPh_3)]^+$ in the crystal of $\mathbf{4}^+PF_6^-\cdot CH_2Cl_2$ showing 30% probability ellipsoids.

b. Oxidized Species. Upon treatment of **4** with NH_4PF_6 in a wet dichloromethane−acetonitrile medium, the color of the solution changes rapidly from dark green to brown red. In this process ring A undergoes selective one-electron oxidation ($abp^{\bullet-} \rightarrow abp$), and the brown-colored monoradical bischelate salt $\mathbf{4}^+PF_6^-$ with the unpaired electron in ring B is isolated from the reaction mixture. This salt is indefinitely stable both in the solid state and in solution. Indeed it is the most stable anion radical complex isolated by us so far. Similar treatment of **5** and **6** with NH_4PF_6 yielded the corresponding nonradical monochelate salts $\mathbf{5}^+PF_6^-$ and $\mathbf{6}^+PF_6^-$, respectively.

It has so far been presumed[5−7] that the oxidation of the chelated anion radicals in dichloromethane−acetonitrile solution containing NH_4PF_6 was caused by oxygen from the air. We have now found that the oxidation process occurs equally smoothly in the absence of oxygen, and the crucial factor is that the solvent mixture must be quite wet. This facilitates acid formation via hydrolysis of NH_4PF_6, the proton then acting as the oxidant: $Ru^{II}L^{\bullet-} + H^+ \rightarrow Ru^{II}L + {}^1/_2H_2$. We have indeed observed that addition of very dilute acids to solutions of the radicals leads to immediate oxidation. This is consistent with the low $E_{1/2}$ of the radicals, vide infra. Significantly, while **4** is smoothly converted to $\mathbf{4}^+$ by this procedure, the latter having a higher $E_{1/2}$ is not oxidized to the nonradical dication $\mathbf{4}^{2+}$.

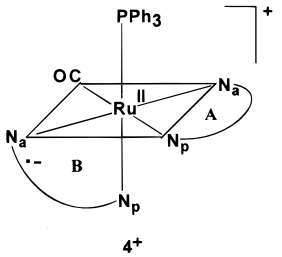

$\mathbf{4}^+$

B. Structures. a. Monoradical BisChelate: Radical Localization. The diradical bischelates **4** did not afford suitable single crystals. The structure of the monoradical $[Ru^{II}(abp)(abp^{\bullet-})(CO)(PPh_3)]PF_6\cdot CH_2Cl_2$, $\mathbf{4}^+PF_6^-\cdot CH_2Cl_2$, has however been determined. A view of the cation is shown in Figure 1, and selected bond parameters are listed in Table 1. The mutually cis CO and PPh_3 ligands both lie trans to pyridine nitrogen atoms while the coordinated azo nitrogen atoms are mutually trans to each other. The chelate ring and the pyridyl ring incorporating N1

(10) Ahmad, N.; Levison, J. J. Robinson, S. D.; Uttley, M. F. *Inorg. Synth.* **1975**, *15*, 45.

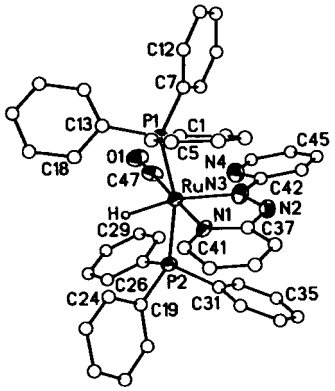

Figure 2. Molecular structure of the cation $[Ru^{II}(abp)(H)(CO)(PPh_3)_2]^+$ in the crystal of $\mathbf{5}^+PF_6^-\cdot H_2O$ showing 30% probability ellipsoids.

Table 1. Selected Bond Distances (Å) and Angles (deg) for $\mathbf{4}^+PF_6^-\cdot CH_2Cl_2$

Ru−P1	2.404(2)	O1−C39	1.125(7)
Ru−C39	1.901(6)	Ru−N1	2.116(4)
Ru−N3	2.013(4)	Ru−N5	2.112(4)
Ru−N7	2.083(4)	N2−N3	1.284(6)
N6−N7	1.336(6)		
C39−Ru−P1	91.5(2)	O1−C39−Ru	173.7(5)
N1−Ru−P1	92.71(12)	N3−Ru−P1	90.30(13)
N5−Ru−P1	174.94(13)	N7−Ru−P1	102.27(13)
N1−Ru−N3	75.1(2)	N1−Ru−N5	83.1(2)
N5−Ru−N7	75.6(2)	N1−Ru−N7	97.7(2)
N3−Ru−N5	91.3(2)	N3−Ru−N7	165.9(2)
C39−Ru−N1	174.6(2)	C39−Ru−N3	101.4(2)
C39−Ru−N5	92.9(2)	C39−Ru−N7	84.8(2)

(ring A) together constitute a good plane with a mean deviation of 0.02 Å, and the pendant pyridyl ring makes a dihedral angle of 24.2° with it. Similarly ring B defines a satisfactory plane (mean deviation 0.04 Å) to which the pendant pyridyl ring incorporating N8 makes a dihedral angle of 15.4°. The dichloromethane molecule does not display any unusual nonbonded interaction in the lattice.

The most remarkable feature of the structure is the difference in the two N−N lengths: N2−N3, 1.284(6) Å (ring A); N6−N7, 1.336(6) Å (ring B). In nonradical and radical monochelates of azo heterocycles, the azo N−N distances have been found to lie in the ranges 1.28−1.29 and 1.33−1.37 Å, approximately corresponding to −N═N− and −N⋯N− descriptions, respectively.[5−7] In the present complex both the types are present within the same molecule, and we have a model case of ground-state radical localization in one of the two rings.

The $Ru-N_p$ lengths, 2.116(4) and 2.112(4) Å, in chelate rings A and B are nearly equal. On the other hand, the corresponding $Ru-N_a$ lengths, 2.013(4) and 2.083(4) Å are well discriminated due to radical localization in ring B. The decrease of Ru−azo back-bonding in going from $Ru^{II}(abp)$ to $Ru^{II}(abp^{\bullet-})$ lengthens the $Ru-N_a$ distance in the latter.

b. Nonradical Monochelates: Isomeric Geometries. The radical chelates **5** and **6** did not afford suitable single crystals, but the nonradical congeners $[Ru^{II}(abp)(H)(CO)(PPh_3)_2]PF_6\cdot H_2O$, $\mathbf{5}^+PF_6^-\cdot H_2O$ and $[Ru^{II}(Clpap)(H)(CO)(PPh_3)_2]PF_6$, $\mathbf{6}^+PF_6^-$, did. Since the radical → nonradical oxidation process occurs under very mild conditions, it is logical to assume that the process is stereoretentive and the gross geometries of **5** and **6** could be ascertained from those of $\mathbf{5}^+$ and $\mathbf{6}^+$. The latter are shown in Figures 2 and 3, and selected bond parameters are given in Table 2. The water molecule in $\mathbf{5}^+PF_6^-\cdot H_2O$ is strongly hydrogen bonded to a neighboring water molecule in the lattice (O...O, 2.54(1) Å). The hydride ligands in $\mathbf{5}^+PF_6^-\cdot H_2O$ and

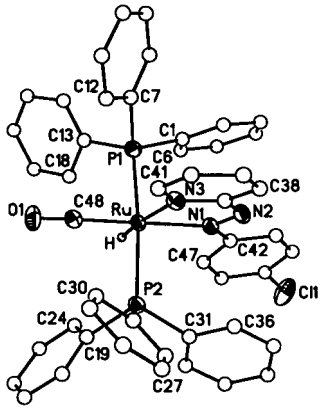

Figure 3. Molecular structure of the cation $[Ru^{II}(Clpap)(H)(CO)(PPh_3)_2]^+$ in the crystal of $\mathbf{6}^+PF_6^-$ showing 30% probability ellipsoids.

$\mathbf{6}^+PF_6^-$ are directly observable in ^1H NMR (vide infra) but are not resolved in difference Fourier maps. The cations $\mathbf{5}^+$ and $\mathbf{6}^+$ have isomeric geometries, the position of H^- and CO ligands being interchanged. The origin of this difference between $\mathbf{5}^+$ and $\mathbf{6}^+$ is unclear.

C. Frontier Orbitals. To gain qualitative insight into the electronic nature of $\mathbf{4}^+$, extended Hückel calculations were performed on the model $[Ru^{II}(abp)(abp^{\bullet-})(PH_3)(CO)]^+$. The half-filled HOMO ($E = -11.04$ eV) and the LUMO ($E = -10.58$ eV) are **7** and **8**, respectively. The former is indeed

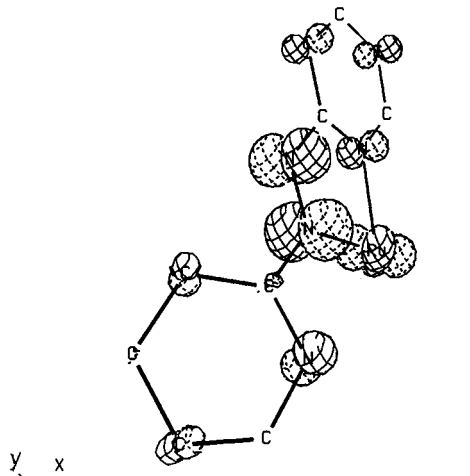

8

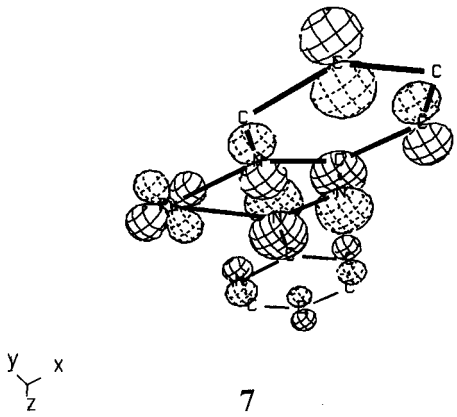

7

localized in ring B and is 51% azo, 19% pyridyl, and 9% metal-d in character. The azo group of ring A makes only a 5% contribution in **7**. On the other hand, **8** is localized on ring A

Table 2. Selected Bond Distances (Å) and Angles (deg) for $\mathbf{5}^{+}PF_6^{-}\cdot H_2O$ and $\mathbf{6}^{+}PF_6^{-}$

	$\mathbf{5}^{+}PF_6^{-}\cdot H_2O$	$\mathbf{6}^{+}PF_6^{-}$		$\mathbf{5}^{+}PF_6^{-}\cdot H_2O$	$\mathbf{6}^{+}PF_6^{-}$
Ru−P1	2.362(3)	2.365(2)	Ru−C47/C48[a]	1.845(12)	1.851(5)
Ru−P2	2.374(3)	2.375(2)	O1−C47/C48[a]	1.138(13)	1.136(6)
Ru−N1	2.105(9)	2.158(4)	N2−N3	1.282(13)	1.285(5)
Ru−N3	2.106(10)	2.127(4)			
P1−Ru−C47/C48[a]	87.3(4)	88.3(2)	N3−Ru−P1	101.3(3)	91.14(11)
P2−Ru−C47/C48[a]	91.8(4)	89.2(2)	N3−Ru−P2	95.6(3)	91.43(11)
N1−Ru−C47/C48[a]	178.1(4)	105.7(2)	P1−Ru−P2	162.77(11)	169.99(5)
N3−Ru−C47/C48[a]	104.9(5)	179.4(2)	N1−Ru−N3	73.9(4)	74.4(2)
N1−Ru−P1	91.5(2)	96.54(11)	O1−C47/C48−Ru[a]	176.70(12)	176.9(5)
N1−Ru−P2	89.8(3)	93.47(11)			

[a] C47 in $\mathbf{5}^{+}PF_6^{-}\cdot H_2O$ and C48 in $\mathbf{6}^{+}PF_6^{-}$.

with 50% azo, 8% pyridyl, and 20% metal-d character. The significantly larger Ru^{II}−abp interaction is no doubt an important factor that places **8** above **7** in energy, causing radical localization.

The orbitals **9** ($E = -8.99$ eV) and **10** ($E = -8.74$ eV) lying ~2 eV above the LUMO are spectrally relevant (see below).

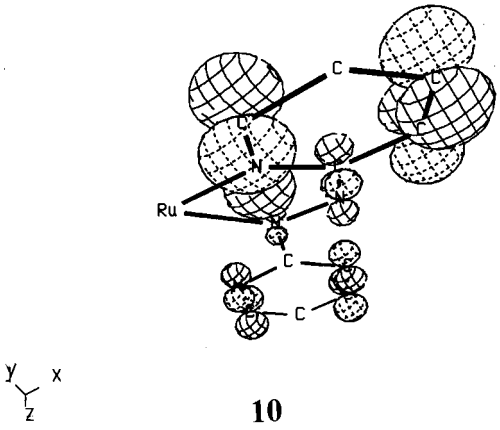

10

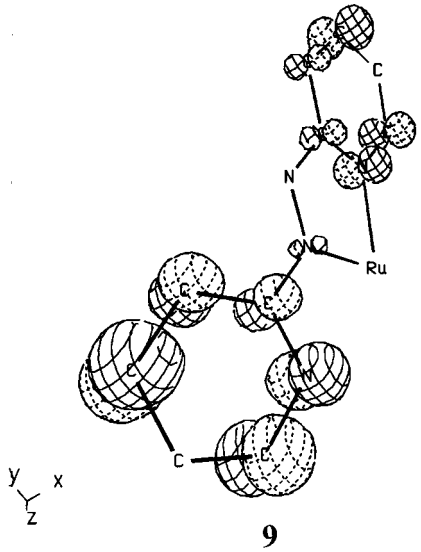

9

These are ~90% pyridyl in character, being localized in rings A and B, respectively. We thus roughly have one pair of azo orbitals (**7** and **8**) and one pair of pyridyl orbitals (**9** and **10**) in the frontier, the energy gap within each pair being relatively small. In monochelate monoradicals of the type $[M^{II}(L^{\bullet-})(X)(CO)(PPh_3)_2]$ (M = Ru, Os; X = Br, Cl), we have single azo and pyridyl orbitals instead.[7,11]

D. Spectra and Reduction Potentials. Relevant data are listed in Table 3 and in the Experimental Section. The radical

Table 3. Electrochemical[a] and IR[b] Data

compd	$E_{1/2}$, V (ΔE_p,[c] mV)	ν_{CO} (cm^{-1})	compd	$E_{1/2}$, V (ΔE_p,[c] mV)	ν_{CO} (cm^{-1})
4	0.10 (100), −0.28 (100)	1960	**5**	−0.46 (100)	1922
$\mathbf{4}^{+}$	0.10 (90), −0.25 (90)	2000	**6**	−0.52 (100)	1910

[a] In CH_2Cl_2 (0.1 M Et_4NClO_4). [b] In a KBr disk. [c] $\Delta E_p = E_{pa} - E_{pc}$.

Table 4. Bulk Magnetic Moments and EPR *g* Values in Solid State

	μ_{eff} (μ_B)	*g* (ΔH_{pp},[a] G)	
compd	298 K	298 K	77 K
4	1.37		
$\mathbf{4}^{+}$	1.79	2.003 (19)	1.999 (13)
5	1.83	2.002 (13)	2.003 (15)
6	1.80	2.002 (9)	2.003 (12)

[a] ΔH_{pp} = peak-to-peak line width.

complexes display one or two moderately intense ($\epsilon = 2500-5500$ M^{-1} cm^{-1}) and relatively broad bands in the 500−600 nm region. In the case of **4** and $\mathbf{4}^{+}$ these are tentatively assigned to intra/interligand transitions **7**, **8** → **9**, **10**. The diamagnetic nonradical species show well-resolved ^1H NMR spectra. The Ru−H proton in $\mathbf{5}^{+}PF_6^{-}$ (−8.79 ppm) and $\mathbf{6}^{+}PF_6^{-}$ (−9.71 ppm) has the expected triplet structure due to coupling with the two ^{31}P atoms of the PPh_3 ligands, the coupling constants being 22.2 and 18.6 Hz, respectively.

The $E_{1/2}$ values of the radical species in dichloromethane solution are listed in Table 3. The monochelates display a single couple due to radical redox $Ru^{II}(L)/Ru^{II}(L^{\bullet-})$. The bischelate shows two successive couples, $Ru^{II}(abp)_2/Ru^{II}(abp)(abp^{\bullet-})$ (electron added to ring B) and $Ru^{II}(abp)(abp^{\bullet-})/Ru^{II}(abp^{\bullet-})_2$ (electron added to ring A), the voltage gap between them being ~0.4 V, which qualitatively correlates with the energy gap between **7** and **8**.

We have noted earlier[5−7] that the PPh_3 and CO ligands play a significant role in radical stabilization, one of the factors being back-bonding. Indeed the CO stretching frequencies of the radicals (Table 3) qualitatively correlate with the azo reduction potentials. The higher the energy of the azo π^*-orbital (lower $E_{1/2}$) the stronger the Ru−CO back-bonding (lower ν_{CO}).

E. Magnetism. a. Monoradicals. The room temperature magnetic moments of the polycrystalline monoradical complexes (Table 4) generally lie near 1.8 μ_B, corresponding to the presence of one unpaired electron ($S = {}^1/_2$). The samples display a strong EPR signal near $g = 2.00$ with peak-to-peak line widths (ΔH_{pp}) in the range 10−20 G (Table 4). The lack of nitrogen hyperfine structure in the EPR spectra is not unusual since the ^{14}N coupling constant in the azo π^* radicals is small and difficult to observe.[1,5−7,12,13]

(11) Shivakumar, M. Ph.D. Thesis, Jadavpur University, Calcutta 700 032, India, February 2000.

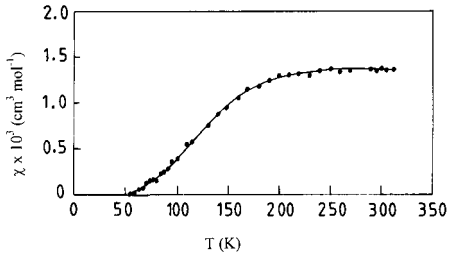

Figure 4. Temperature dependence of the molar susceptibility χ for complex **4**. The solid line represents the fit with $J = -299$ cm^{-1}.

b. Diradical 4. The effective magnetic moment of **4** is ~1.4 μ_B at room temperature. The susceptibility decreases progressively with temperature, and the sample becomes virtually diamagnetic near 50 K (Figure 4). The observed behavior is reproduced well on the basis of antiferromagnetic interaction between the two radical sites, the coupling constant J defining the singlet−triplet energy gap as -299 cm^{-1}. It is logical to assume that the two half-filled shells in **4** are closely similar to those in **7** and **8**. The significant metal-d character (vide supra) of these orbitals ensures a metal-mediated pathway for the magnetic interaction. Pure samples of complex **4** are EPR-silent, presumably due to relaxation phenomena.

We note that complex **4** can be considered as a distant analogue of bissemiquinone complexes of the type $[Ru^{II}(sq^{\bullet -})_2(PPh_3)_2]$[14,15] and $[Ru^{II}(sq^{\bullet -})_2(CO)_2]$.[16] In the latter, the antiferromagneticinteraction is however much stronger and the species are diamagnetic at room temperature.

Concluding Remarks

The scope of the synthesis of radical anion chelates via heterolytic M−H bond cleavage by azo heterocyclic ligands (L) has been augmented by using the dihydridic starting material $[Ru^{II}(H)_2(CO)(PPh_3)_3]$, **3**. Both steps of the conversion $Ru^{II}(H)_2 \rightarrow Ru^{II}(H)(L^{\bullet -}) \rightarrow Ru^{II}(L^{\bullet -})_2$ have been realized in the case of L = abp; for L = Clpap, only the first step could be diagnosed. The hydridic monoradicals $[Ru^{II}(abp^{\bullet -})(H)(CO)(PPh_3)_2]$, **5**, and $[Ru^{II}(Clpap^{\bullet -})(H)(CO)(PPh_3)_2]$, **6**, are curiously isomeric in coordination geometry. The oxidations such as **4** $\rightarrow$ **4**$^+$, **5** $\rightarrow$ **5**$^+$, and **6** $\rightarrow$ **6**$^+$ are brought about by acids (H^+).

The diradical bischelate $[Ru^{II}(abp^{\bullet -})_2(CO)(PPh_3)]$, **4**, displays strong metal-mediated antiferromagnetism, and upon oxidation to the monoradical **4**$^+$, the unpaired electron with ~40% azo π^*-character gets localized in one of the chelate rings. This is consistent with simple molecular orbital computations.

The role of CO in stabilizing the radical species is reflected in the qualitative correlation between CO stretching frequencies and radical $E_{1/2}$.

Experimental Section

Starting Materials and Solvents. The azo-2,2′-bipyridine and 2-(*p*-chlorophenylazo)pyridine ligands were synthesized according to previously published procedures.[17,18] The starting material **3** was prepared by the reported procedure.[10] 2-Aminopyridine (Aldrich), $RuCl_3 \cdot xH_2O$ (Arora-Mathey, India), and NH_4PF_6 (Aldrich) were used as received. Benzene and heptane used in synthesis were dried by distillation over Na/benzophenone. The purification of dichloromethane and the preparation of tetraethylammonium perchlorate (TEAP) for electrochemical work were done as described before.[19,20]

Physical Measurements. Spectral measurements were made with the following equipment: UV−vis, Shimadzu UV-1601 PC spectrophotometer; IR (KBr disk), Perkin-Elmer 783 spectrometer; ^{1}H NMR, Bruker 300 MHz FT spectrometer; X-band EPR, Varian E-109C spectrometer fitted with a liquid nitrogen quartz dewar, 9.1−9.2 GHz microwave frequency, 100 kHz modulation, 30 dB power, 3300 G sweep center, 1000 G sweep width, 240 s sweep time. Electrochemical measurements were performed under a nitrogen atmosphere using a PAR 370-4 electrochemistry system as before:[20] working electrode, planar Beckmann model 39273 platinum-inlay electrode; auxiliary electrode, platinum wire; reference electrode, SCE; supporting electrolyte, Et_4NClO_4 (0.1 M); scan rate, 50 mV s^{-1}; solution concentration, ~10^{-3} M. All potentials reported are uncorrected for junction contributions.

Room temperature magnetic moments were measured by using a PAR-155 vibrating sample magnetometer. Variable temperature susceptibility work was done with a Georges Associates Inc. Lewis-coil force magnetometer equipped with a closed cycle cryostat (Air Products) and a Cahn-2000 balance (we are thankful to Professor A. R. Chakravarty for the use of the equipment). The antiferromagnetically coupled susceptibility in the diradical $[Ru^{II}(abp^{\bullet -})_2(CO)(PPh_3)]$, **4**, was fitted to the expression of eq 4, where J is the singlet−triplet separation and the other symbols have their usual meaning.[21]

$$\chi = 2Ng^2\beta^2/kT[3 + \exp(-J/kT)] \qquad (4)$$

Preparation of Complexes. $[Ru^{II}(abp^{\bullet -})_2(CO)(PPh_3)]$, 4. Azo-2,2′-bipyridine (60 mg, 0.33 mmol) was dissolved in 10 mL of dry benzene, and the solution was purged with dry nitrogen for 0.5 h. To this solution was added $[Ru^{II}(H)_2(CO)(PPh_3)_3]$, **3** (100 mg, 0.11 mmol), and the mixture was heated to reflux under nitrogen for 40 min. The color of the reaction mixture changed from yellow to dark green. The solution was allowed to cool to room temperature and then evaporated to dryness under reduced pressure, affording a dark-colored solid which was repeatedly extracted with warm dry heptane until the heptane extracts were no longer deep green in color. The combined heptane extract was concentrated to a volume of 15 mL under reduced pressure. The solution was kept in the refrigerator overnight. The precipitated solid was filtered, washed with dry acetonitrile, and dried immediately in vacuo. Yield: 58 mg (71%). Data for **4** are as follows. Anal. Calcd for $C_{39}H_{31}N_8OPRu$: C, 61.65; H, 4.08; N, 14.75. Found: C, 60.96; H, 4.18; N, 14.54. UV−vis (C_6H_6) [λ_{max}, nm (ϵ, M^{-1} cm^{-1})]: 568 (4250), 368 (13 950).

$[Ru(abp^{\bullet -})(H)(CO)(PPh_3)_2]$, 5. To a solution of abp (26 mg, 0.14 mmol) dissolved in dry benzene (20 mL) was added **3** (75 mg, 0.08 mmol), and the reaction mixture was heated to reflux under nitrogen for 1 h. The resulting dark green solution was allowed to cool somewhat and then quickly evaporated to

(12) Pal, C. K.; Chattopadhyay, S.; Sinha, C. R.; Chakravorty, A. *Inorg. Chem.* **1994**, *33*, 6140.
(13) Pal, C. K.; Chattopadhyay, S.; Sinha, C. R.; Chakravorty, A. *Inorg. Chem.* **1996**, *35*, 2442.
(14) Bhattacharya, S.; Pierpont, C. G. *Inorg. Chem.* **1991**, *30*, 1511.
(15) Bag, N.; Lahiri, G. K.; Basu, P.; Chakravorty, A. *J. Chem. Soc., Dalton Trans.* **1992**, 113.
(16) Bhattacharya, S.; Pierpont, C. G. *Inorg. Chem.* **1994**, *33*, 6038.
(17) Goswami, S.; Chakravarty, A. R.; Chakravorty, A. *Inorg. Chem.* **1981**, *20*, 2246.
(18) Baldwin, A.; Lever, A. B. P.; Parish, R. V. *Inorg. Chem.* **1969**, *8*, 107.
(19) Lahiri, G. K.; Bhattacharya, S.; Ghosh, B. K.; Chakravorty, A. *Inorg. Chem.* **1987**, *26*, 4324.
(20) Chandra, S. K., Basu, P.; Ray, D.; Pal, S.; Chakravorty, A. *Inorg. Chem.* **1990**, *29*, 2423.
(21) Kahn, O. *Molecular Magnetism*; Wiley-VCH: New York, 1993, p 104.

Table 5. Crystallographic Data for $\mathbf{4}^{+}PF_6^{-}\cdot CH_2Cl_2$, $\mathbf{5}^{+}PF_6^{-}\cdot H_2O$ and $\mathbf{6}^{+}PF_6^{-}$

	$\mathbf{4}^{+}PF_6^{-}\cdot CH_2Cl_2$	$\mathbf{5}^{+}PF_6^{-}\cdot H_2O$	$\mathbf{6}^{+}PF_6^{-}$
empirical formula	$C_{40}H_{33}Cl_2F_6N_8OP_2Ru$	$C_{47}H_{41}F_6N_4O_2P_3Ru$	$C_{48}H_{39}ClF_6N_3OP_3Ru$
fw	989.7	1001.8	1016.6
space group	$P2_1/c$ (No. 14)	$P2_1/n$ (No. 14)	$P2_1/n$ (No. 14)
a, Å	14.174(6)	9.433(2)	10.496(5)
b, Å	16.451(4)	38.914(17)	22.389(8)
c, Å	18.381(4)	13.084(3)	19.720(6)
β, deg	98.00(3)	103.47(2)	90.53(3)
V, Å^3	4244(2)	4670(2)	4634(3)
Z	4	4	4
temp, K	295	295	295
λ, Å	0.7107	0.7107	0.7107
ρ_{calc}, g cm^{-3}	1.551	1.427	1.461
μ, cm^{-1}	0.641	0.505	0.564
$R1$,[a] $wR2$[b] [$I>2\sigma(I)$]	0.0578, 0.1461	0.0828, 0.2049	0.0471, 0.1170

[a] $R1 = \sum||F_o| - |F_c||/\sum|F_o|$. [b] $wR2 = [\sum w(F_o^2 - F_c^2)^2/\sum w(F_o^2)^2]^{1/2}$.

dryness while still warm. The resulting solid was quickly extracted several times with warm heptane. The heptane extract was reduced to a volume of 10 mL under reduced pressure. The solid, which precipitated from the concentrated solution on standing, was filtered, washed with dry acetonitrile, and dried immediately. Yield: 14 mg (20%). Data for **5** are as follows. Anal. Calcd for $C_{47}H_{39}N_4OP_2Ru$: C, 67.30; H, 4.65; N, 6.68. Found: C, 67.14; H, 4.73; N, 6.48. UV−vis (C_6H_6) [λ_{max}, nm (ϵ, M^{-1} cm^{-1})]: 577 (5350), 540 (5550).

[Ru^{II}(Clpap$^{\bullet-}$)(H)(CO)(PPh$_3$)$_2$], 6. The synthesis of this complex is similar to that of **5**, Clpap replacing abp. The reactant stoichiometry was Clpap (32 mg, 0.15 mmol) and **3** (75 mg, 0.08 mmol). Yield: 19 mg (27%). Data for **6** are as follows. Anal. Calcd for $C_{48}H_{39}ClN_3OP_2Ru$: C, 66.08; H, 4.47; N, 4.82. Found: C, 65.87; H, 4.39; N, 4.77. UV−vis (C_6H_6) [λ_{max}, nm (ϵ, M^{-1} cm^{-1})]: 600 (3170), 560 (3190).

[Ru^{II}(abp)(abp$^{\bullet-}$)(CO)(PPh$_3$)]PF$_6$, $\mathbf{4}^{+}PF_6^{-}$. In this and subsequent syntheses the solvents were not dry. To a solution of [Ru^{II}(abp$^{\bullet-}$)$_2$(CO)(PPh$_3$)] (50 mg, 0.07 mmol) in dichloromethane (10 mL) was added an acetonitrile (10 mL) solution of NH_4PF_6 (20 mg, 0.12 mmol). The mixture was magnetically stirred in air. The dark green color of the solution immediately turned brown-red. Stirring was continued for 0.5 h. The excess solvent was removed under reduced pressure, and the resultant solid was washed with water repeatedly and dried in vacuo. Subsequent chromatographic workup of the dichloromethane solution of the solid on a silica gel column with a 1:4 acetonitrile−toluene mixture as the eluant afforded the brown-colored complex. The solid was recrystallized from a dichloromethane−hexane mixture yielding $\mathbf{4}^{+}PF_6^{-}\cdot CH_2Cl_2$, which was dried in vacuo, leading to loss of the solvent of crystallization. Yield: 39 mg (65%). Data for $\mathbf{4}^{+}PF_6^{-}$ are as follows. Anal. Calcd for $C_{39}H_{31}F_6N_8OP_2Ru$: C, 51.76; H, 3.43; N, 12.39. Found: C, 51.68; H, 3.39; N, 12.31. UV−vis (CH_2Cl_2) [λ_{max}, nm (ϵ, M^{-1} cm^{-1})]: 556 (sh, 2660), 489 (3100), 349 (10 880).

[Ru^{II}(abp)(H)(CO)(PPh$_3$)$_2$]PF$_6$, $\mathbf{5}^{+}PF_6^{-}$. The dark-colored complex was prepared in the same manner as $\mathbf{4}^{+}PF_6^{-}$. Chromatographic workup yielded a violet-colored eluate with a 1:2 acetonitrile−toluene mixture. On evaporation under reduced pressure, a dark-violet-colored crystalline solid was obtained. Yield: 30 mg (52%). Data for $\mathbf{5}^{+}PF_6^{-}$ are as follows. Anal. Calcd for $C_{47}H_{39}F_6N_4OP_3Ru$: C, 57.37; H, 3.97; N, 5.69. Found: C, 57.20; H, 3.87; N, 5.61. UV−vis (CH_2Cl_2) [λ_{max}, nm (ϵ, M^{-1} cm^{-1})]: 555 (3300), 354 (9970). IR (KBr, cm^{-1}): 1960 cm^{-1} (ν_{CO}). ^{1}H NMR ($CDCl_3$, 298 K, ppm from TMS): δ 8.84 (d, $J = 4.5$, 1H), 8.37 (d, $J = 7.9$, 1H), 8.01 (t, $J = 7.7$, 1H), 7.85 (d, $J = 7.7$, 2H), 7.74 (t, $J = 8.1$, 1H), −8.79 (t, $J = 22.2$, 1H).

[Ru^{II}(Clpap)(H)(CO)(PPh$_3$)$_2$]PF$_6$, $\mathbf{6}^{+}PF_6^{-}$. The complex was prepared in a manner similar to that of $\mathbf{5}^{+}PF_6^{-}$. Chromatographic workup yielded a light-green-colored eluate with a 1:2 acetonitrile−toluene mixture which on evaporation under reduced pressure gave a green-colored crystalline solid. Yield: 34 mg (58%). Data for $\mathbf{6}^{+}PF_6^{-}$ are as follows. Anal. Calcd for $C_{48}H_{39}ClF_6N_3OP_3Ru$: C, 56.67; H, 3.84; N, 4.13. Found: C, 56.53; H, 3.71; N, 4.06. UV−vis (CH_2Cl_2) [λ_{max}, nm (ϵ, M^{-1} cm^{-1})]: 600 (1870), 450 (sh, 4500), 400 (18 300). IR (KBr, cm^{-1}): 1955 cm^{-1} (ν_{CO}). ^{1}H NMR ($CDCl_3$, 298 K, ppm from TMS): δ 8.81 (d, $J = 5.7$, 1H), 8.34 (d, $J = 7.9$, 1H), 8.08 (t, $J = 7.6$, 1H), 7.82 (d, $J = 8.9$, 2H), 7.43 (t, $J = 6.5$, 1H), 6.91 (d, $J = 9.1$, 2H), −9.71 (t, $J = 18.6$, 1H).

Molecular Orbital Calculation. Extended Hückel calculations were performed using the ICON software package developed by Hoffmann and others.[22−25] The calculations were performed using experimental atomic coordinates transformed to rectangular axes using the program SHELXTL (Version 5.03).[26] The PPh_3 group in the molecule was simplified to PH_3 via replacement of Ph by H, the P−H bond lengths were adjusted to 1.42 Å, and the angles around P were left unchanged.

In a previous calculation[7] on [Os(pap$^{\bullet-}$)(Br)(CO)(PPh$_3$)$_2$] (pap = 2-(phenylazo)pyridine), the pendant pap Ph as well as the phosphine Ph were replaced by H and the geometry of the coordination sphere was also adjusted for higher symmetry; experimental coordinates were not used. This yielded a HOMO with 70% azo character. It is more realistic to use experimental coordinates as has been done in the present work. On the basis of the experimental coordinates,[5] the EHMO results[11] on [Ru(pap$^{\bullet-}$)(Cl)(CO)(PH$_3$)$_2$] are as follows. The half-filled HOMO is 52% azo, 7% pyridyl, 13% phenyl, and 15% metal-d, and the LUMO is 90% pyridyl and 3% azo. Use of the approximations as in the osmium compound[7] pushes the azo contribution to a much higher value.

X-ray Structure Determination. Single crystals (dimension of sides 0.2−0.4 mm) of complexes were grown by slow diffusion of hexane into dichloromethane solutions of the complexes. Cell parameters were determined by the least-squares fit of 30 machine-centered reflections ($2\theta = 14-30°$). Data were collected by the ω-scan technique in the range $3° \le 2\theta \le 48°$

(22) Hoffmann, R. *J. Chem. Phys.* **1963**, *39*, 1397.
(23) Ammeter, J. H.; Bürgi, H.-B.; Thibeault, J. C.; Hoffmann, R. *J. Am. Chem. Soc.* **1978**, *100*, 3686.
(24) Maelli, C.; Proserpio, D. M. CACAO, Version 4.0, Firenze, Italy, July 1994.
(25) Maelli, C.; Proserpio, D. M. *J. Chem. Educ.* **1990**, *67*, 399.
(26) Sheldrick, G. M. SHELXTL, Version 5.03, Structure Determination Software Programs, Siemens Analytical X-ray Instruments Inc., Madison, WI, 1994.

for $4^+PF_6^-\cdot CH_2Cl_2$, $3° \le 2\theta \le 45°$ for $5^+PF_6^-\cdot H_2O$ (relatively poorly diffracting), and $3° \le 2\theta \le 47°$ for $6^+PF_6^-$ on a Siemens R3m/V four-circle diffractometer with graphite-monochromated Mo Kα ($\lambda = 0.710\,73$ Å) radiation at 25 °C. Two check reflections after each 198 reflections showed no intensity reduction for any of the crystals. All data were corrected for Lorentz-polarization effects and absorption.[27] Totals of 7940 ($4^+PF_6^-\cdot CH_2Cl_2$), 6754 ($5^+PF_6^-\cdot H_2O$), and 7686 ($6^+PF_6^-$) were collected, 6689, 6084, and 6877, respectively, of which were unique; of these 5192, 4249, and 5408 were taken as observed ($I > 2\sigma(I)$).

All calculations for data reduction and structure solution and refinement were done using the programs of SHELXTL, Version 5.03.[26] The structures were solved by full-matrix least-squares on F^2, making non-hydrogen atoms anisotropic. The hydridic H atoms in $5^+PF_6^-\cdot H_2O$ and $6^+PF_6^-$ were fixed at a distance of 1.70 Å[28−31] from the metal center. In $5^+PF_6^-\cdot H_2O$, 28 of the total 39 hydrogen atoms could be located. All the hydrogen atoms in $6^+PF_6^-$ were directly located from X-ray data. For $4^+PF_6^-\cdot CH_2Cl_2$ all the hydrogen atoms were included at calculated positions. The N atoms of the pendant pyridyl ring of the chelated abp ligands in $4^+PF_6^-\cdot CH_2Cl_2$ and $5^+PF_6^-\cdot H_2O$ were identified by the bond lengths, the average C−N and C−C distances being 1.33 and 1.37 Å, respectively. Significant crystal data are listed in Table 5.

Acknowledgment. Financial support received from the Indian National Science Academy, the Department of Science and Technology, and the Council of Scientific and Industrial Research, New Delhi, is acknowledged. Thanks are due to Professor A. R. Chakravarty and Mr. Sibaprasad Bhattacharyya for help in measurements and computations. Affiliation with the Jawaharlal Nehru Centre for Advanced Scientific Research, Bangalore, is acknowledged.

Supporting Information Available: X-ray crystallographic files in CIF format, for the structure determinations of $4^+PF_6^-\cdot CH_2Cl_2$, $5^+PF_6^-\cdot H_2O$, and $6^+PF_6^-$. This material is available free of charge via the Internet at http://pubs.acs.org.

IC000356B

(27) North, A. C. T.; Philips, D. C.; Mathews, F. S. *Acta Crystallogr.* **1968**, *24A*, 351.
(28) Pramanik, A.; Bag, N.; Chakravorty, A. *J. Chem. Soc., Dalton Trans.* **1992**, 97.
(29) Skapski, A. C.; Stephens, F. A. *J. Chem. Soc., Dalton Trans.* **1974**, 390.
(30) McConway, A. C.; Skapski, A. C.; Phillips, L.; Young, R. J.; Wilkinson, G. *J. Chem. Soc., Chem. Commun.* **1974**, 327.
(31) Ashworth, T. V.; Nolte, M. J.; Singleton, E.; Laing, M. *J. Chem. Soc., Dalton Trans.* **1977**, 1816.